

Global dust density in two-dimensional complex plasma

Yi-Zhen Zhao(赵逸真), Song-Fen Liu(刘松芬), Wei Kong(孔伟), and Fang Yang(杨芳)

Citation: Chin. Phys. B, 2024, 33 (**6**): 065201. DOI: 10.1088/1674-1056/ad2a76
Journal homepage: http://cpb.iphy.ac.cn; http://iopscience.iop.org/cpb

What follows is a list of articles you may be interested in

Distribution of charged lunar dust in the south polar region of the moon

Qing Xia(夏清), Ming-Hui Cai(蔡明辉), Liang-Liang Xu(许亮亮), Rui-Long Han(韩瑞龙), Tao Yang(杨涛), and Jian-Wei Han(韩建伟)
Chin. Phys. B, 2022, 31 (**4**): 045201. DOI: 10.1088/1674-1056/ac2e61

Directional motion of dust particles at different gear structuresin a plasma

Chao-Xing Dai(戴超星), Chao Song(宋超), Zhi-Xiang Zhou(周志向), Wen-Tao Sun(孙文涛), Zhi-Qiang Guo(郭志强), Fu-Cheng Liu(刘富成), Ya-Feng He(贺亚峰)
Chin. Phys. B, 2020, 29 (**2**): 025203. DOI: 10.1088/1674-1056/ab6109

Dust charging and levitating in a sheath of plasma containing energetic particles

Jing Ou(欧靖), Xiao-Yun Zhao(赵晓云), Bin-Bin Lin(林滨滨)
Chin. Phys. B, 2018, 27 (**2**): 025204. DOI: 10.1088/1674-1056/27/2/025204

Experimental and modeling researches of dust particles in the HL-2A tokamak

Huang Zhi-Hui (黄治辉), Yan Long-Wen (严龙文), Tomita Yukihiro (冨田幸博), Feng Zhen (冯震), Cheng Jun (程钧), Hong Wen-Yu (洪文玉), Pan Yu-Dong (潘宇东), Yang Qing-Wei (杨青巍), Duan Xu-Ru (段旭如), HL-2A Team
Chin. Phys. B, 2015, 24 (**2**): 025204. DOI: 10.1088/1674-1056/24/2/025204

Kadomtsev–Petviashvili equation for dust ion-acoustic solitons in pair-ion plasmas

Hafeez Ur-Rehman
Chin. Phys. B, 2013, 22 (**3**): 035202. DOI: 10.1088/1674-1056/22/3/035202

Global dust density in two-dimensional complex plasma

Yi-Zhen Zhao(赵逸真)[1], Song-Fen Liu(刘松芬)[1,†], Wei Kong(孔伟)[2,‡], and Fang Yang(杨芳)[2]

[1] *School of Physics, Nankai University, Tianjin* 300071, *China*
[2] *College of Science, Civil Aviation University of China, Tianjin* 300300, *China*

(Received 25 December 2023; revised manuscript received 2 February 2024; accepted manuscript online 19 February 2024)

The driven-dissipative Langevin dynamics simulation is used to produce a two-dimensional (2D) dense cloud, which is composed of charged dust particles trapped in a quadratic potential. A 2D mesh grid is built to analyze the center-to-wall dust density. It is found that the local dust density in the outer region relative to that of the inner region is more nonuniform, being consistent with the feature of quadratic potential. The dependences of the global dust density on equilibrium temperature, particle size, confinement strength, and confinement shape are investigated. It is found that the particle size, the confinement strength, and the confinement shape strongly affect the global dust density, while the equilibrium temperature plays a minor effect on it. In the direction where there is a stronger confinement, the dust density gradient is bigger.

Keywords: dust particles, quadratic potential, two-dimensional mesh grid

PACS: 52.27.Lw, 52.27.Gr, 52.65.–y **DOI:** 10.1088/1674-1056/ad2a76

1. Introduction

Complex (dusty) plasma shares a number of similarities with other many-body systems such as colloidal suspension. The nanometer to millimeter charged dust particles behave in a gaseous-like, liquid-like, or solid-like state depending on the relative value of the kinetic energy to the effective interparticle potential energy. To obtain the generic properties of the system, such as transport,[1–14] microscopic structure,[15–26] and collective oscillation,[27–35] a cluster composed of a finite number of particles is often employed in the simulation, and the boundary condition is assumed to be periodic. In that way, the unbounded system is simply regarded as infinite. However, a horizontal confinement that is used to prevent the charged dust particles from diffusing into the wall of the container is needed in most of the dusty plasma experiments. For example, an electrode with a shallow circular parabolic trough is devised in the experiment of Melzer *et al.*[36,37] The resultant trap gives rise to a radically inward force, which can be anisotropic by changing the relative strength of the trap at different direction. In the experiment of Lin *et al.*,[38] a hollow coaxial cylinder is put on the bottom electrode to confine the charged dust particles. By adjusting the rf power, a very thick outward radial space charge field is generated and the negatively charged dust particles are confined in the central uniform region. The system size shrinks or expands depending on the rf power. In another of their experiments,[39] a rectangular confining cell with 14.5 mm width, 30 mm length, and 14 mm height is placed at the center of the bottom electrode surface to confine the charged dust particles. The cluster with an elongated cross section is observed. This experiment has significance in that one can create a two-dimensional (2D) dusty plasma with a bigger length scale at the preferred direction, which facilitates the investigation of linear waves with longer wave-length and the subsequent turbulence. In the experiment of Morfill *et al.*,[40] a copper ring with inner diameter of 40 mm and height of 2 mm is placed on the rf electrode. It introduces a horizontal confining potential and the charged dust particles can be pushed towards the center. In the experiments of Piel *et al.*[41] and Goree *et al.*,[42] a spherical depression at the center of the electrode surface is designed to provide a radial confinement for the charged dust particles. In the experiment of Thomas *et al.*,[43] the researchers use a strong magnetic field to modify the confinement by changing the dynamics of electrons, ions, and even the charged dust particles. So far, it has been known that the interplay between the charged dust particles and the confinement does play an important role in the appearance of the system. In this paper, we attempt to answer one basic, while fundamentally important question: how does the global density of the charged dust particles, from the inner to the outer, respond to the confinement? This study has a potential application to spectroscopy, imaging, and understanding of dust-associated waves. For example, it has been shown that the dispersion of linear dust-acoustic waves is modified by the dust density nonuniformity.[44] In the study of photonic crystal, Shukla *et al.*[45] and Hartmann *et al.*[46] have suggested that an external magnetic field affects the interparticle spacing of superparamagnetic charged dust particles, and hence the density of the system. Correspondingly, the dust crystal as a tunable filter in the terahertz regime (the interparticle distance on the order of 100 mm) is expected.

†Corresponding author. E-mail: lsfnku@nankai.edu.cn
‡Corresponding author. E-mail: wkong@cauc.edu.cn

© 2024 Chinese Physical Society and IOP Publishing Ltd

Early experiment has shown that the mean interparticle separation increases up to about 10% in the range $0.7R < r < R$ for the hundreds of mm-sized particles (Fig. 5 therein),[38] where R is the radius of the circular cluster. The method used for determining the interparticle separation is to measure the first peak of the radial distribution function (RDF). However, the accuracy of RDF relies on the uniformity of the objects being processed. In a recent experiment conducted by Killer *et al.*,[47] the researchers studied the three-dimensional (3D) dust distribution in dust clouds of both micro- and sub-micro-sized particles using a tomographic method. They found that the dust density of both micro-dusts and nano-dusts changes a lot from the inner region to the outer region (up to several times). Basically, the configuration of the cluster is due to the superposition of confinement, equilibrium temperature, particle number, particle size, and so on. These mixed effects are rather difficult to be distinguished in the experiment. Here, we investigate the dependences of the global dust density on equilibrium temperature, particle size, confinement strength, and confinement shape separately, with the purpose of having an insight into the physical mechanism behind them. The confinement is assumed to be quadratic, which is popular in many dusty plasma experiments. The global dust density of the system is analyzed in a Lagrange framework, where each particle is weighted onto the 2D mesh grids.

This paper is arranged as follows. Section 2 gives the simulation model in detail. The simulation results and discussion are presented in Section 3. Section 4 is devoted to a conclusion.

2. Simulation model

In a 2D bounded cluster composed of identically charged dust particles, the Hamiltonian of the system is given by

$$H = \sum_{i=1}^{N}\left(\frac{\boldsymbol{p}_i^2}{2m} + \Phi_{\rm c}\right) + \sum_{i\neq j}^{N}\Phi_{\rm Y}, \tag{1}$$

where the first term, second term, and third term of right hand side of Eq. (1), respectively, correspond to kinetic energy, confinement potential energy, and interaction potential energy of the system. N is the number of charged dust particles, and $\boldsymbol{p}_i$ is the momentum of the i-th charged dust particle. Due to the screening effect of background plasma, $\Phi_{\rm Y}$ takes the form of Yukawa potential energy $(Q^2/r)\exp(-r/\lambda_{\rm D})$, where Q is the charge on each dust particle, r is the interparticle distance, and $\lambda_{\rm D}$ is the Debye length of the system. Two confinements with different shapes including circle and ellipse are considered. For the circular one, $\Phi_{\rm c}$ is written as $m_i\omega^2\boldsymbol{r}_i^2/2$, where m_i and $\boldsymbol{r}_i$ are the dust mass and position vector of the i-th particle, respectively. ω is set by the shape of the cavity in the lower electrode. In simulations, ω also refers to the strength of the confinement. For the elliptical one, $\Phi_{\rm c}$ is written as $m_i\omega^2(\alpha x_i^2 + y_i^2)/2$, where α is a dimensionless parameter which determines the aspect ratio of the ellipse, x_i and y_i are the coordinates of the i-th charged dust particle. To reach the desirable temperature, a driven-dissipative thermostat is used to sustain the equilibrium of the system. For the term of dissipative force, it reads $-\nu m\boldsymbol{v}_i(t)$, where ν is the collision frequency between the charged dust particles and the neutral gas, and $\boldsymbol{v}_i(t)$ is the velocity of the i-th particle at time t. For the term of driven force, it reads $\zeta_i(t)$, which relates to the temperature of the system in terms of fluctuation-dissipation theorem[41–44]

$$\langle\zeta_i(0)\zeta_i(t)\rangle = 2m\nu k_{\rm B}T\delta(t), \tag{2}$$

where $k_{\rm B}$ is the Boltzmann constant, T is the equilibrium temperature of the system, and δ is the Dirac delta function.

We aim to analyze the global dust density of the confined system on an equal footing by building a uniform $N_x \times N_y$ mesh grid in real space. Supposing a homogenous system (no confinement) with a given density n_0 consists of N charged dust particles, then the averaging weight $w_0 = \sum w(l,k)/(N_xN_y)$ can be calculated, where $w(l,k)$ is the particle-related weight on each mesh grid (l together with k, ranging from 1 to 30, determine the identity of individual mesh grid). Basically, $w(l,k) \simeq w_0$ is independent of l and k for the homogenous system in equilibrium. When the confinement is present, the edge of the system tends to bend and the cluster shrinks. The charged dust particles rearrange themselves, causing the updated weight $w(l,k)$ to strongly depend on l and k. In physics, $w(l,k)$ reflects the local field that the dust particles are experiencing. We recalculate $w(l,k)$ on each mesh grid, and the global dust density of the confined system is expressed by $(w(l,k)/w_0)n_0$, a value based on the initial given density n_0. The interparticle spacing of the confined system is smaller than that of the unbounded system in the region where $w(l,k)/w_0 > 1$, and vice versa. Noting that $w(l,k) = 0$ corresponds to the region where the particle is absent.

The normalizations for this study are as follows: length is scaled by $a = (n_0\pi)^{-1/2}$, which is the Wigner–Seitz radius of the homogenous system with number density n_0. Time is scaled by the inverse nominal plasma frequency $\omega_{\rm pd}^{-1}$ of the unbounded system, where $\omega_{\rm pd} = (2Q_0^2/(a^3m_0))^{1/2}$.[48–51] Energy is normalized by $U_0 = Q_0^2/a$. Q_0 and m_0 are the typical values in experiments of dusty plasma. For example, Q_0 ranges from 10^3e to 10^4e,[52,53] where e is the elementary charge. For silica, melamine formaldehyde, and aluminium oxide, m_0 is on the order of 10^{-18} kg to 10^{-7} kg depending on its size.[43,54–57] Screening coefficient κ is one of the most important parameters characterizing the thermodynamics of the system. In order to separate the effects of κ and ω on the

global dust density (since the mean interparticle distance relates to the confinement strength), we define the screening coefficient by $\kappa = a/\lambda_D$ instead of the conventional one, i.e., the ratio of mean interparticle distance to Debye length. In this way, one of κ and ω can be studied when the other is fixed.

Initially, the charged dust particles with a Gaussian distribution are randomly loaded in the x–y plane. The first 2×10^5 time steps are used to relax the system. In the next 10^5 time steps, the position of each charged dust particle is sampled at an interval of 10 time steps. To reduce the statistical error, the global dust density of the system $w(l,k)$ is derived by averaging 10^4 ensembles. The typical parameters used in the simulation are as follows: the screening coefficient κ of the system ranges from 1 to 5, the collision frequency ν (in units of ω_{pd}) between neutral gas and charged dust particles is from 0.01 to 0.1,[15,58–61] the system temperature T (in units of U_0) changes from 0.1 to 0.005,[62–65] and the confinement strength ω (in units of ω_{pd}) varies from 0.1 to 0.25. Upon the previous study that the modification of Yukawa potential by including the particle size brings minor effects on the dynamics of the system,[45] we infer that the effect of the particle size on the global dust density mainly stems from Q and m of the particles. Here, Q and m are changed proportionally, i.e., $\mu = Q/Q_0 = m/m_0$. We note that all of the other parameters are kept constant when one of the parameters is investigated.

3. Simulation result and discussion

The simulations are arranged as follows. In Subsection 3.1, the dependence of $w(l,k)/w_0$ on equilibrium temperature T is investigated. Based on this, we proceed with the next simulation with a fixed T. In Subsection 3.2, the effects of the particle size on the global density are calculated inspired by recent experiments.[39,46] In Subsection 3.3, $w(l,k)/w_0$ as a function of ω is studied. Intuitively, the system size should shrink with increasing ω due to the stronger confinement. On the other hand, how the global dust density changes accordingly is not yet clear. In Subsection 3.4, the global dust density with an anisotropic confinement is discussed. We note that the ion drag force is omitted in this model, thus a void-free cluster is expected.

3.1. Effects of equilibrium temperature on global dust density

Figure 1 shows $w(l,k)/w_0$ as a function of R, where R refers to the radial distance from the center to the boundary of the cluster, and the confinement has a circular shape. Different equilibrium temperatures, including $T = 0.005$, 0.01, 0.02, and 0.1, are considered, which correspond to the coupling constant of the system $\Gamma = Q^2/(ak_BT) = 200$, 100, 50, and 10, respectively. According to the reference,[47] a 2D one-component infinite Yukawa system with $\kappa = 1$ melts near $\Gamma = 170$. This suggests that our investigation covers the liquid-like state basically. It is found that: (1) the global dust density has a radial-symmetric distribution, being consistent with the shape of the confinement (as shown in Fig. 4(a)). The value of $w(l,k)/w_0 > 1$ indicates that the confinement strongly increases the dust density due to the shrinking of the cluster. (2) By analyzing the slope of the curves, one finds that the global dust density near the boundary changes more than that of the inner region, i.e., having a bigger gradient. This also can be explained by the shape of the confinement used here, i.e., the potential farther away from the center is steeper. (3) The global dust density basically remains unchanged for the cases of lower temperature ($T = 0.02$, 0.01, 0.005). However, the system with a higher temperature ($T = 0.1$) tends to extend due to the stronger mobility of the charged dust particles, and the global dusty density has a slight change correspondingly.

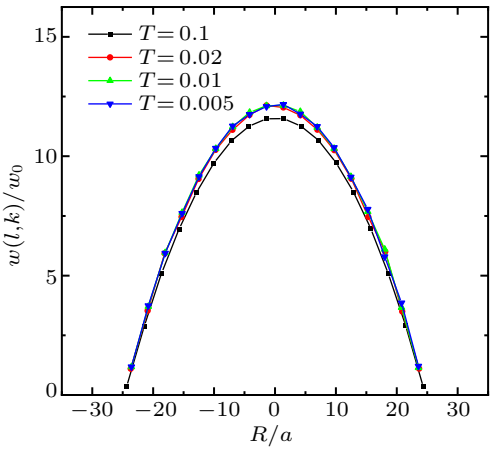


Fig. 1. The $w(l,k)/w_0$ as a function of R, the equilibrium temperatures are set to be $T = 0.005$, 0.01, 0.02, and 0.1, respectively.

3.2. Effects of particle size on global dust density

Due to the feasibility of individual particle tracking, the micron-sized dusts are frequently used in the experiments to study the strong-coupling related phenomena. While in the technological plasma, the nanoparticles are of great interest for their better flexibility and controllability. On this point, the problem related to particle size deserves to be paid attention. Here we investigate the effects of particle size on the global density of the system. Figure 2 shows $w(l,k)/w_0$ as a function of R, where $\mu = 1$, 3, 5, and 7. We choose $T = 0.1$ for the stronger mobility of the system. Note that Fig. 1 has already shown that the global dust density of the system is independent of T, therefore we expect the conclusions obtained here are also applicable to the cases of $T = 0.02$, 0.01, and 0.005.

It is found that the global density, particularly the central density decreases with a saturation trend when μ is increased. Meanwhile, the boundary of the system extends. In addition, one finds that the global density of the system tends to be

more uniform with increasing μ by observing the slope of the curves. These results can be explained as follows: when the charge and mass of the particles increase proportionally, the electrostatic interparticle interaction ($\sim (\mu Q)^2$) gains more increment relative to that of the confinement force ($\sim$ μm), hence the cluster tends to expand due to the relatively stronger Coulomb repelling, and the global density tends to be more uniform due to the relatively weaker confinement. Killer *et al.* in their experiment (Figs. 3 and 4 therein) have demonstrated that the charged particles have a radial-dependent density in the horizontal plane near the upper edge of the 3D dust cloud.[47] In fact, the particles with bigger size ($a_d = 1.78$ μm, where a_d is the radius of the dust) have a relatively more uniform density distribution, while the particles with smaller size ($a_d = 210$ nm) have a relatively nonuniform density distribution. Our simulations shown here are basically consistent with their experiment.

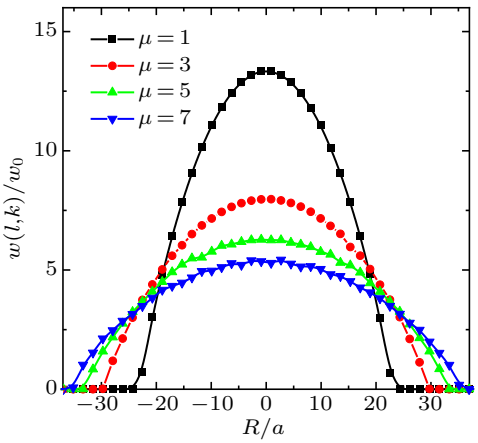


Fig. 2. The $w(l,k)/w_0$ as a function of R, where $\mu = 1, 3, 5, 7$.

3.3. Effects of confinement strength on global dust density

Figure 3 shows $w(l,k)/w_0$ as a function of R, where different confinement strengths are used, including $\omega = 0.1, 0.15, 0.2, 0.25$. As expected, the dust cloud shrinks with increasing confinement strength. Meanwhile, the dust particles are more uniform along the radial direction as ω decreases. This makes sense because the potential well tends to be flatter when ω decreases. Additionally, we are interested in the variation of the dust density at different R when ω is changed.

Here we analyze only the region where the dust particles always appear, i.e., $R \leq 20$ approximately. As shown in the inset of Fig. 3, it is found that the dust density at the center of cluster decreases linearly as ω is increased, while this dependence turns to be nonlinear far away from the center, for example, when $R = 13.5$. All of these findings suggest that the confinement strength plays an important role in the dust density. It is believed that detailed dependence of the global density is also related to the confinement shape, as discussed in the next subsection.

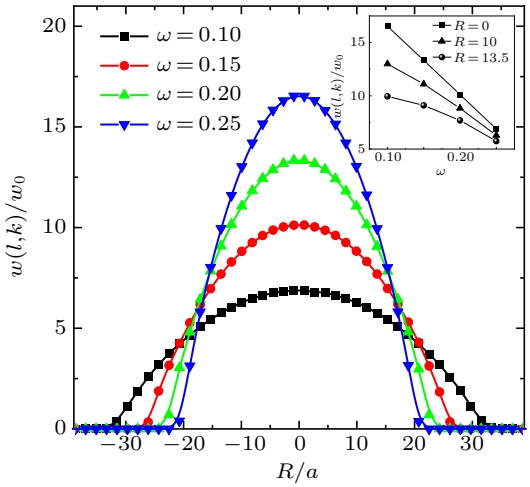


Fig. 3. The $w(l,k)/w_0$ as a function of R, with different confinement strengths $\omega = 0.1, 0.15, 0.2, 0.25$.

3.4. Effects of confinement shape on global dust density

To investigate the effects of confinement shape on the global dust density, the circular quadratic confinement is deformed by adjusting the parameter α, i.e., $\Phi_c = m_i\omega^2(\alpha x_i^2 + y_i^2)/2$. This idea has been proposed in the previous studies.[36,37] As shown in Fig. 4, we give the 3D plot of the gradually-deformed quadratic potential, where $\alpha = 1.0$, 0.8, 0.6, and 0.4, respectively. It is found that the cylindrical-symmetric potential well ($\alpha = 1.0$) tends to be anisotropic as α is decreased. For the case of $\alpha = 0.4$, the potential has an obvious sinking along the x-direction, which relaxes the x-direction confinement of the dust particles to some extent, even leads to the escape event when the kinetic energy of the system is sufficiently strong.

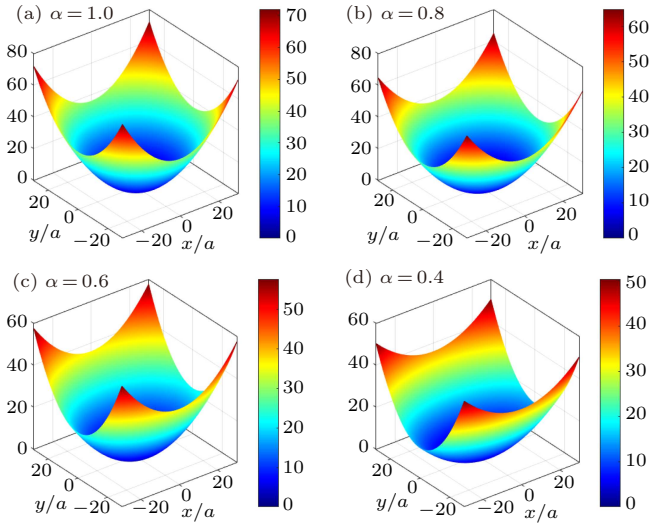


Fig. 4. The 3D plot of the gradually-deformed quadratic potential, where $\alpha = 1.0, 0.8, 0.6, 0.4$ respectively.

It is noted that the potential at the y-direction also declines with decreasing α, thus the dust particles' motion along the y-direction should be affected as well. Figure 5 shows the corresponding global dust density with different α. Being consistent with those of Fig. 4, the dust cloud extends at

the x-direction due to the weaker confinement, and shrinks at the y-direction to match the shape of the confinement.

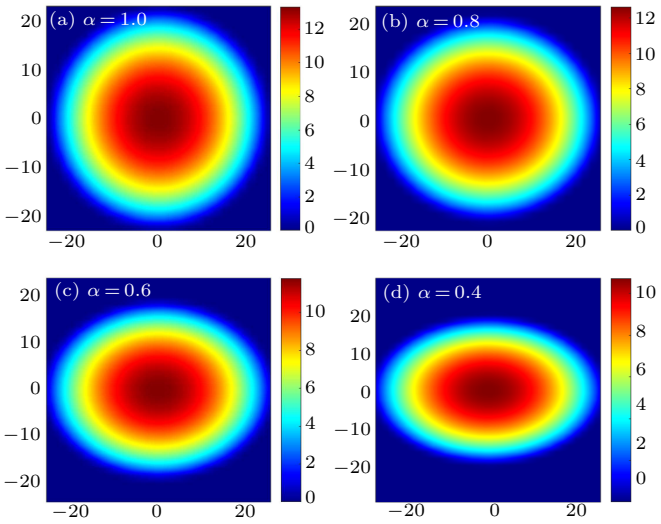


Fig. 5. Global dust density with different α.

In addition, one can observe that the peak density in the central region is decreased. This trend can be verified clearly by analyzing the radial dust density along x-direction and y-direction, respectively, as shown in Fig. 6.

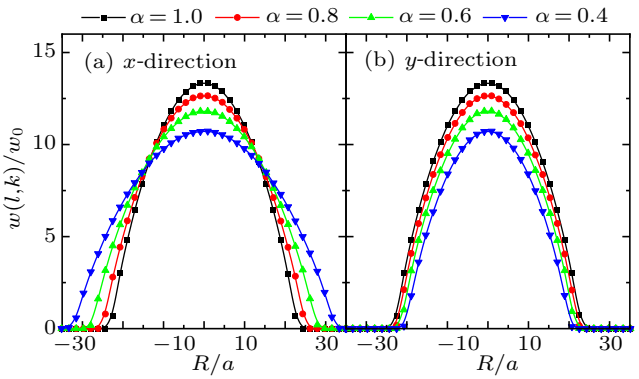


Fig. 6. The $w(l,k)/w_0$ as a function of R in the x-direction and the y-direction, respectively.

It is found that both of the peak densities along the two directions decrease with decreasing α. At the x-direction, the boundary of the system extends; while at the y-direction, the boundary of the system is suppressed slightly, being consistent with those of Fig. 5. It is noted that the dust density at the y-direction has a bigger gradient relative to that of the x-direction when α is much smaller than 1. Meanwhile, we believe that this conclusion will be reversed if α is much bigger than 1. In other words, the dust density is bigger in the direction where there is a stronger confinement. This point can also be confirmed by Fig. 3.

4. Conclusion

The dust density nonuniformity has been observed in previous complex plasma experiments. However, how the global dusty density responds to the confinement is not clear to the best of our knowledge. In this work, we first use the Langevin dynamics simulation to produce a 2D dense dust cloud trapped in a quadratic potential. We then build a mesh grid and perform an analysis of the radial density with respect to a number of factors including equilibrium temperature, particle size, confinement strength, and confinement shape. It is found that the particle size, the confinement strength, and the confinement shape, relative to the equilibrium temperature, have important effects on the global dusty density. In addition, we find that the dust density gradient is stronger in the direction where there is a stronger confinement. These conclusions hold for different particle numbers (N ranging from 1600 to 10000 has been examined) and neutral collision frequencies. This study provides a helpful understanding of the appearance of 2D trapped dense clouds. It also gives a reference for future studies considering dust density nonuniformity.

Acknowledgements

Project supported by the National Natural Science Foundation of China (Grant Nos. 12275354 and 11805272) and the Civil Aviation University of China (Grant No. 3122023PT08).

References

[1] Juan W T, Chen M H and I L 2001 *Phys. Rev. E* **64** 016402
[2] Lai Y J and I L 2002 *Phys. Rev. Lett.* **89** 155002
[3] Liu B and Goree J 2008 *Phys. Rev. Lett.* **100** 055003
[4] Ott T, Bonitz M, Donkó Z and Hartmann P 2008 *Phys. Rev. E* **78** 026409
[5] Kong W, Liu S F, Hu B L and Wang L 2009 *Phys. Rev. E* **80** 036406
[6] Donkó Z, Goree J, Hartmann and Liu B 2009 *Phys. Rev. E* **79** 026401
[7] Hou L J, Piel A and Shukla P K 2009 *Phys. Rev. Lett.* **102** 085002
[8] Ott T, Bonitz M and Hartmann P 2009 *Phys. Rev. Lett.* **103** 099501
[9] Hou L J, Mišković Z L, Piel A and Shukla P K 2009 *Phys. Plasmas* **16** 053705
[10] Liu B and Goree J 2014 *Phys. Plasmas* **21** 063704
[11] Feng Y, Goree J, Liu B, Intrator T P and Murillo M S 2014 *Phys. Rev. E* **90** 013105
[12] Yang F, Kong W, Liu S F, Shi F and Wang Y P 2017 *Phys. Plasmas* **24** 063702
[13] Du C R, Nosenko V, Thomas H M, Lin Y F, Morfill G E and Ivlev A V 2019 *Phys. Rev. Lett.* **123** 185002
[14] Yang F, Liu S F, Kong W and Li Y L 2019 *Phys. Plasmas* **26** 113701
[15] Thomas H, Morfill G E, Demmel V, Goree J, Feuerbacher B and Möhlmann D 1994 *Phys. Rev. Lett.* **73** 652
[16] Chu J H and I L 1994 *Phys. Rev. Lett.* **72** 4009
[17] Fortov V E, Ivlev A V, Khrapak S A, Khrapak A G and Morfill G E 2005 *Phys. Rep.* **421** 1
[18] Liu Y H, Chew L Y and Yu M Y 2008 *Phys. Rev. E* **78** 066405
[19] Löwen H, Oguz E C, Assoud L and Messina R 2012 *Adv. Chem. Phys.* **148** 225
[20] Morfill G E and Ivlev A V 2009 *Rev. Mod. Phys.* **81** 1353
[21] Donko Z, Hartmann P and Kalman G J 2009 *J. Phys.: Conf. Ser.* **162** 012016
[22] Thomas E Jr, Konopka U, Merlino R L and Rosenberg M 2015 *Phys. Plasmas* **22** 030701
[23] Kong W, Yang F, Liu S F and Shi F 2016 *Phys. Plasmas* **23** 103705
[24] Thomas E Jr, Konopka U, Merlino R L and Rosenberg M 2016 *Phys. Plasmas* **23** 055701
[25] Block D and Melzer A 2019 *J. Phys. B: At. Mol. Opt. Phys.* **52** 063001

[26] Yang F, Kong W, Liu S F and Wang C Z 2020 *Phys. Rev. E* **102** 043213
[27] Homann A, Melzer A, Peters S and Piel A 1997 *Phys. Rev. E* **56** 7138
[28] Nunomura S, Goree J, Hu S, Wang X, Bhattacharjee A and Avinash K 2002 *Phys. Rev. Lett.* **89** 035001
[29] Kalman G J, Hartmann P, Donkó Z and Rosenberg M 2004 *Phys. Rev. Lett.* **92** 065001
[30] Nunomura S, Zhdanov S, Samsonov D and Morfill G 2005 *Phys. Rev. Lett.* **94** 045001
[31] Piel A and Goree J 2006 *Phys. Plasmas* **13** 104510
[32] Nosenko V, Goree J and Piel A 2006 *Phys. Rev. Lett.* **97** 115001
[33] Hartmann P, Donkó Z, Kalman G J and Kutasi K 2005 *Phys. Rev. E* **72** 026409
[34] Hou L J, Shukla P K, Piel A and Mišković Z L 2009 *Phys. Plasmas* **16** 073704
[35] Kong W, Yang F, Liu S F and Shi F 2018 *Phys. Plasmas* **25** 083709
[36] Melzer A, Buttenschön B, Miksch T, Passvogel M, Block D, Arp O and Piel A 2016 *Plasma Sources Sci. Technol.* **25** 055004
[37] Melzer A, Krüger H, Schütt S and Mulsow M 2019 *Phys. Plasmas* **26** 093703
[38] Juan W T, Huang Z H, Hsu J W, Lai Y J and I L 1998 *Phys. Rev. E* **58** 6947(R)
[39] Wang Y C, Juan W T and I L 2000 *Phys. Rev. E* **62** 5667
[40] Konopka U, Morfill G E and Ratke L 2000 *Phys. Rev. Lett.* **84** 891
[41] Schablinski J, Block D, Piel A, Melzer A, Thomsen H, Kahlert H and Bonitz M 2012 *Phys. Plasmas* **19** 013705
[42] Goree J, Liu B and Feng Y 2013 *Plasma Phys. Control. Fusion* **55** 124004
[43] Thomas E Jr, Merlino R L and Rosenberg M 2012 *Plasma Phys. Control. Fusion* **54** 124034
[44] Asaduzzaman M, Mamun A A and Ashrafi K S 2011 *Phys. Plasmas* **18** 113704
[45] Rosenberg M, Sheehan D P and Shukla P K 2006 *Phys. Rev. E* **34** 490
[46] Hartmann P, Kalman G J, Donkó Z and Bakshi P 2011 *Phys. Rev. E* **84** 016409
[47] Killer C, Greiner F, Groth S, Tadsen B and Melzer A 2016 *Plasma Sources Sci. Technol.* **25** 055004
[48] Kalman G J, Hartmann P, Donko Z and Rosenberg M 2004 *Phys. Rev. Lett.* **92** 065001
[49] Feng Y, Goree J, Liu B, Intrator and Murillo M S 2014 *Phys. Rev. E* **90** 013105
[50] Yang F, Kong W, Liu S F, Shi F and Wang Y P 2017 *Phys. Plasmas* **24** 063702
[51] Kong W, Liu S F, Yang F, Shi F and Wang Y P 2017 *Phys. Plasmas* **25** 083709
[52] Vasiliev M M, Dyachkov L G, Antipov S N, Huijink R, Petrov O F and Fortov V E 2011 *Europhys. Lett.* **93** 15001
[53] Romero-Talamas C A, Bates E M, Birmingham W J and Rivera W F 2016 *IEEE Trans. Plasma Sci.* **44** 535
[54] Feng Y, Goree J and Liu B 2010 *Phys. Rev. Lett.* **105** 025002
[55] Bonitz M, Kählert H, Ott T and Löwen H 2013 *Plasma Sources Sci. Technol.* **22** 015007
[56] Hartmann P, Donko Z, Ott T, Kählert H and Bonitz M 2013 *Phys. Rev. Lett.* **111** 155002
[57] Haralson Z and Goree J 2017 *Phys. Rev. Lett.* **118** 195001
[58] Feng Y, Goree J, Liu B and Cohen E G D 2011 *Phys. Rev. E* **84** 046412
[59] Fortov V E, Nefedov A P, Torchinsky V M, Molotkov V I, Petrov O F, Samarian A A, Lipaev A M and Khrapak A G 1997 *Phys. Lett. A* **229** 317
[60] Feng Y, Goree J, Liu B, Intrator and Murillo M S 2014 *Phys. Rev. E* **90** 013105
[61] Intrator T P, Dorf L, Sun X, Feng Y, Sears J and Weber T 2014 *Phys. Plasmas* **21** 042109
[62] Feng Y, Liu B and Goree J 2008 *Phys. Rev. E* **78** 026415
[63] Klumov B A and Morfill G E 2009 *JETP Letters* **90** 444
[64] Yang F, Kong W, Liu S F and Li Y L 2020 *Phys. Plasmas* **27** 113702
[65] Hartmann P, Donkó Z, Kalman G J and Kutasi K 2005 *Phys. Rev. E* **72** 026409